Determining Noise Temperatures in Beam Waveguide Systems

W. Imbriale, W. Veruttipong, T. Otoshi, and M. Franco
Ground Antennas and Facilities Engineering Section

A new 34-m research and development antenna was fabricated and tested as a precursor to introducing beam waveguide (BWG) antennas and Ka-band (32 GHz) frequencies into the NASA/JPL Deep Space Network. For deep space use, system noise temperature is a critical parameter. There are thought to be two major contributors to noise temperature in a BWG system: the spillover past the mirrors and the conductivity loss in the walls. However, to date, there are no generally accepted methods for computing noise temperatures in a beam waveguide system. An extensive measurement program was undertaken to determine noise temperatures in such a system along with a correspondent effort in analytic prediction. Utilizing a very sensitive radiometer, noise temperature measurements were made at the Cassegrain focus, an intermediate focal point, and the focal point in the basement pedestal room. Several different horn diameters were used to simulate different amounts of spillover past the mirrors. Two analytic procedures were developed for computing noise temperature, one utilizing circular waveguide modes and the other a semiempirical approach. The results of both prediction methods are compared to the experimental data.

I. Introduction

Noise temperature due to a beam waveguide (BWG) system is one of the major contributors to antenna-receive system noise, especially for an ultralow noise system or a system with high spillover power in the BWG shroud. A reasonably accurate prediction of the BWG noise temperature is essential. Direct analytical computation of the noise temperature of elaborate BWG systems, including all mirrors, is an extremely complex problem and, to date, there is no generally accepted method. This article presents two new techniques, one a purely analytical method and the second a semiempirical approach.

The analytical method extends the approach of [1], which computes the waveguide modes that are propagating in the oversized waveguides. Reference [1] describes a physical optics (PO) integration procedure of the currents on the BWG mirrors using a Green's function appropriate to the circular waveguide geometry. Once all the modes in the waveguide are known, it is a simple matter to use stan-

dard approximations to determine the attenuation constant and, thus, the conductivity loss if the conductivity of the wall material is known. Also, all energy that propagates toward, but spills past, a BWG mirror is assumed to be lost in the walls of the BWG as well. The noise temperature is computed assuming both loss components see ambient temperature.

The second method uses a technique that combines an analytical approach with data from measurements to construct a specific expression to compute the BWG noise temperature.

To validate both approaches, a series of measurements were made on DSS 13, the recently completed research and development 34-m BWG antenna (see Figs. 1 and 2). The experiments consisted of making very accurate noise temperature measurements for different gain horns located at both the Cassegrain focus (f1) and the BWG focus of the upper portion of the BWG system (f2) (designed to image the horn at the Cassegrain optics focal point). This portion of the BWG optics is enclosed in a 2.44-m-diameter tube. By taking measurements at both focal points, the noise temperature of the BWG portion of the optics can be accurately determined. The results of both computation methods are compared to the measured data.

II. Waveguide Mode Theory

The BWG tube analysis is conceptually similar to the PO analysis used in reflector antenna analysis. Currents induced in the BWG mirror are obtained using a standard PO approximation of $J = 2\hat{n} \times H_{inc}$ where $\hat{n}$ is the surface normal and H_{inc} is the incident field. However, this analysis differs in the methods by which the incident field on a mirror and the scattered field are calculated.

One approach to calculating the scattered field is to use a dyadic Green's formulation [1] where the field scattered from a BWG mirror is computed using the Green's function appropriate to the cylindrical waveguide geometry.

While it is conceptually convenient to use Green's functions to discuss the comparison with PO, the actual computation using this approach is rather cumbersome. Instead, a simpler method is used to calculate waveguide fields, based upon the reciprocity theorem. The basic problem is to find the fields radiated by an arbitrary current (the PO currents on the reflector) in a cylindrical waveguide. The problem is easily solved by expanding the radiated field in terms of a suitable set of normal modes with amplitude coefficients determined by an application of the Lorentz reciprocity theorem.

An arbitrary field in a waveguide can be represented as an infinite sum of the normal modes for the guide. Let the normal modes be represented by

$$\overline{E}_n^{(\pm)} = (\overline{e}_n \pm \overline{e}_{zn})\, e^{\mp \Gamma_n z}$$
$$\overline{H}_n^{(\pm)} = (\pm \overline{h}_n + \overline{h}_{zn})\, e^{\mp \Gamma_n z} \tag{1}$$

where $\overline{E}_n^{(+)}$ represents a mode traveling in the $+z$ direction and $\overline{E}_n^{(-)}$ is a mode traveling in the $-z$ direction. For a basic normal mode description, see [2].

Let the field radiated in the $+z$ direction by the current be represented by

$$\overline{E}^{(+)} = \sum_n a_n \overline{E}_n^{(+)}$$
$$\overline{H}^{(+)} = \sum_n \frac{a_n}{Z_n} \overline{H}_n^{(+)} \tag{2}$$

and the field radiated in the $-z$ direction by

$$\overline{E}^{(-)} = \sum_n b_n \overline{E}_n^{(-)}$$
$$\overline{H}^{(-)} = \sum_n \frac{b_n}{Z_n} \overline{H}_n^{(-)} \tag{3}$$

Recalling the Lorentz reciprocity theorem, if $\overline{E}_1$, $\overline{H}_1$ and $\overline{E}_2$, $\overline{H}_2$ are the fields due to $\overline{J}_1$, $\overline{J}_2$, respectively, then

$$\int_s \hat{n} \bullet \left[\overline{E}_1 \times \overline{H}_2 - \overline{E}_2 \times \overline{H}_1\right] ds =$$
$$\int_v \left[\overline{E}_2 \bullet \overline{J}_1 - \overline{E}_1 \bullet \overline{J}_2\right] dV \tag{4}$$

If we let $\overline{E}_1$, $\overline{H}_1$ be the fields due to the sources J and $\overline{E}_n^{(\pm)}$, and $\overline{H}_n^{(\pm)}$ be the modal (source-free) solutions, substituting in the Lorentz reciprocity theorem gives

$$-\int_s \left[\overline{E}_n^{(\pm)} \times \overline{H}_1 - \overline{E}_1 \times \frac{\overline{H}_n^{(\pm)}}{Z_n}\right] \bullet \hat{n} ds = \int_v \overline{E}_n^{(\pm)} \bullet J dV \tag{5}$$

If we choose a volume bounded by the perfectly conducting guide walls and the two cross-sectional planes S_1 and S_2 (see Fig. 3), then

$$\int_s = \int_{s_1} (-\hat{z}) \bullet \left[\overline{E}^{(-)} \times \frac{\overline{H}_n^{(\pm)}}{Z_n} - \overline{E}_n^{(\pm)} \times H^{(-)}\right] ds$$

$$+ \int_{s_2} (\hat{z}) \bullet \left[\overline{E}^{(+)} \times \frac{\overline{H}_n^{(\pm)}}{Z_n} - \overline{E}_n^{(\pm)} \times H^{(+)}\right] ds \tag{6}$$

Note that the integral along the wall does not contribute because on S_3 $\hat{n} \bullet \overline{E}_1 \times \overline{H}_2 = \overline{H}_2 \bullet \hat{n} \times \overline{E}_1 = \overline{H}_2 \bullet$ tangential $\overline{E} = 0$ for either $E^{(\pm)}$ or $E_n^{(\pm)}$.

Also only transverse fields enter into computations because $\hat{z} \bullet \overline{E} \times \overline{H}$ selects transverse components.

For the normal mode function E_n^+, H_n^+, it is readily found that

$$\int_s = -\frac{2b_n}{Z_n} \tag{7}$$

when the expansion for E^+ and E^- are used in conjunction with the orthogonal property and

$$\int_s (\overline{e}_n \times \overline{h}_m) \bullet \hat{z} ds = \begin{cases} 0 \text{ if } n \neq m \\ 1 \text{ if } m = n \end{cases} \tag{8}$$

Also, if we use the normal mode function $\overline{E}_n^{(-)}$, $\overline{H}_n^{(-)}$, we find that

$$\int_s = -2\frac{a_n}{Z_n} \tag{9}$$

We have therefore shown that

$$a_n = -\frac{1}{2} Z_n \int_v \left[\overline{E}_n^{(-)} \bullet \overline{J}\right] dV$$

$$b_n = -\frac{1}{2} Z_n \int_v \left[\overline{E}_n^{(+)} \bullet \overline{J}\right] dV \tag{10}$$

Since we have only surface currents, the integral for the PO currents is over the surface of the reflector. If we let

$$c_n = -\frac{1}{2} \int_s J_s \bullet \overline{E}_n^{(-)} ds \tag{11}$$

where J_s is the PO currents on the mirror, then

$$\overline{H}^+ = \sum_n c_n \overline{H}_n^{(-)}$$

$$\overline{E}^+ = \sum_n Z_n c_n \overline{E}_n^{(-)} \tag{12}$$

and the total power contained in the fields is

$$P = \sum_n Z_n |c_n|^2 \tag{13}$$

If the spillover past the mirror is small (i.e., >25 dB edge taper), the PO currents induced on the first mirror are computed in the standard way, by utilizing the free-space near-field radiating H field of the horn and $J_s = 2\hat{n} \times H_{inc}$. Or they may be computed by utilizing a technique similar to the one just described to compute the propagating modes from the horn, radiating in the oversized waveguide and utilizing the appropriate H field derived from these modes as the incident field. On subsequent mirrors, PO currents are computed from the H field derived from the propagating waveguide modes. The technique is summarized in Fig. 4, where it should be noted that

$$H = \int_s \overline{J}_1 \bullet \overline{\overline{G}}_{wg} ds = \sum_n c_n \overline{H}_n^{(-)} \tag{14}$$

Power loss in the conductor is obtained utilizing the standard technique to compute the power dissipated in the conductor per unit length [2] as

$$P_d(Z) = R \int_0^{2\pi} |\overline{H}_t|^2 \, a d\phi \tag{15}$$

where

$$R = \sqrt{\frac{\omega\mu}{2\sigma}} \tag{16}$$

and σ is the wall conductivity, a the radius, and $|\overline{H}_t|^2$ the tangential H field. It should be noted that P_d is a function of Z since $|\overline{H}_t|^2$ is a function of Z (i.e., it is composed of more than one waveguide mode).

Power loss is computed from

$$P = P_o e^{-2\alpha d} \tag{17}$$

where d is the distance from Z_1 to Z_2 and the attenuation constant is computed as

$$\alpha d = \frac{\int_{Z_1}^{Z_2} P_d(z)dz}{2P_f} \tag{18}$$

where P_f is the power flow in the waveguide.

To compute noise temperature, it is convenient to separate the total RF power originating from the horn aperture (viewed in transmission, for convenience) and propagating into two parts

$$P_{BWG} = P_m + P_{spill} \tag{19}$$

where P_{spill} is the portion that spills past the mirrors (since the mirrors do not fill the waveguide). P_{spill} can be computed for each mirror by integrating the total power radiated from the induced mirror currents and comparing it to the incident power. Note that the computation uses the induced currents derived from the waveguide modes. It is then assumed that this spillover power sees ambient temperature since it would be lost in the tube due to multiple bounces in a lossy material.

The total noise temperature then is composed of two parts—the noise due to the spillover power added to the noise from the attenuation of P_m due to the conductivity loss.

III. Semiempirical Approach

The noise temperature of elaborate BWG systems, including mirrors and shroud, can also be computed by using a new technique that combines an analytical approach with data from measurement tests to construct a specific expression. This technique begins by separating total RF power into two parts; that is, the power that originates from a horn aperture and propagates through a BWG shroud (P_{BWG}) (see Fig. 5) is separated by

$$P_{BWG} = P_m + P_{spill} \tag{20}$$

where P_m is the majority of the total power that is always confined inside all BWG mirrors. P_m does not contact the BWG wall and there are no multiple reflection, diffraction, and creeping wave components. P_m can be computed easily and accurately because all BWG wall and mirror interactions are not included. In this analysis, mirrors are assumed to radiate in free space, making the P_{spill} different from the P_{spill} of the waveguide mode theory. P_{spill} is the sum of spillover powers of each mirror. It creeps and bounces around the BWG walls, mirrors, brackets (behind the mirrors), and edges, and suffers dissipation loss and consequent noise. On an average, the P_{spill} power largely dissipates before a small remainder exits the BWG opening near f1 (see Fig. 2). Even though P_{spill} can be computed accurately ($P_{spill} = P_{BWG} - P_m$), its field distribution and its chaotic behavior inside the lossy BWG is virtually impossible to compute analytically.

From Eq. (20), the corresponding noise temperatures are

$$T_{BWG} = T_m + T_{spill} \tag{21}$$

where T_{BWG} is the total noise temperature (in kelvins) due to the BWG system (including the shroud, mirror, brackets, etc.). The values T_m and T_{spill} are the noise temperature contributions from P_m and P_{spill}, respectively. Because of the simplicity of P_m, its corresponding noise temperature T_m can be computed with acceptable accuracy. For 6061T6 aluminum with conductivity of 2.3×10^7 S/m and a 270-K physical temperature, the noise temperature T_m at X-band (8.45 GHz) [3] is

$$T_m = 0.734\frac{P_m}{P_{BWG}} = 0.734\alpha_m \tag{22}$$

where α_m is the P_m fraction of P_{BWG}, dimensionless.

The noise temperature due to spillover power P_{spill} is given in a very simple form as

$$T_{spill} = \left(\frac{P_1}{P_{BWG}}\right)T_1 + \left(\frac{P_2}{P_{BWG}}\right)T_2 = \alpha_1 T_1 + \alpha_2 T_2 \tag{23}$$

where P_1 is the total spillover power of the two mirrors (M5 and M6) in the basement and the value P_2 is the total spillover power of the four mirrors (M1, M2, M3, and M4) above the basement ceiling. The values α_1 and α_2 are the

normalized powers (with respect to P_{BWG}) of P_1 and P_2, respectively.

By substituting Eqs. (22) and (23) into Eq. (21), the BWG noise temperature at X-band becomes

$$T_{BWG} = 0.734\alpha_m + \alpha_1 T_1 + \alpha_2 T_2 \tag{24}$$

By performing various measurements at the NASA DSN BWG research station at Goldstone, the coefficients T1 and T2 at X-band have been obtained [3].

$$\text{No basement shroud} \quad \begin{matrix} T_1 = 300 \pm 10\,\text{K} \\ T_2 = 240 \pm 45\text{K} \end{matrix} \tag{25}$$

$$\text{Full shroud} \quad \begin{matrix} T_1 = 280 \pm 20\,\text{K} \\ T_2 = 230 \pm 45\,\text{K} \end{matrix} \tag{26}$$

Figure 6 shows the comparison between predicted and measured BWG noise temperatures for various total spillover powers at X-band. The results indicate a very good agreement, especially in the operating range (0.5 percent $\leq P_{spill} \leq$ 1.2 percent).

IV. Measurements Program

Figure 1 shows a recent photograph of the 34-m-diameter BWG antenna at the NASA/JPL Goldstone tracking facility near Barstow, California. It is the first BWG antenna built for NASA and is primarily intended for research and development. One of its uses has been to develop and verify theoretical models that can be used as tools for designing future improved BWG antennas.

Focal points f1, f2, and f3 are depicted in Fig. 2. Focal point f1 is the Cassegrain focal point near the main reflector vertex. An intermediate focal f2 lies above the azimuth track, and f3 is the final BWG focal point located in a subterranean pedestal room. Degradations caused by the BWG system mirrors and shrouds were determined from comparisons made of operating system noise temperatures measured at the different focal points.

As discussed earlier, the goal of the experimental technique was to determine the degradations caused by noise temperature contributions from wall losses and mirror spillovers in the BWG system. The experimental technique that was conceived and implemented involved measuring operating system noise temperature at f1, f2, and f3. The difference between noise temperatures at f1 and f2 gives information on total losses from the BWG system that include (1) dissipative losses due to finite conductivity of four mirrors, (2) spillover losses associated with four mirrors, and (3) shroud wall losses between f1 and f2. Similarly, information about total losses from the remaining two mirrors, shroud walls, and unshrouded path between f2 and f3 are determined by measuring the difference in noise temperatures at those focal points.

To obtain information on losses pertaining only to the Cassegrain portion of the BWG antenna, the experimental procedure involved measuring operating system noise temperature with the test package on the ground, and then with the test package installed at f1. The difference between f1 and ground noise temperatures reveals the amount of degradation caused by spillover of power from the horn into the region between the subreflector and main reflector, scattering from the tripod legs, noise contribution from illumination of the ground and sky region as seen from the subreflector focus, and leakage through gaps between panels and perforations in the main reflector surfaces, as well as noise temperature due to illuminating the area between the horn aperture and BWG shroud walls.

To yield the information described above, the experiment required that absolute noise temperature at the different test locations be accurate to about ± 0.5 K and be repeatable to about ± 0.2 K. The accuracy of values obtained for differential measurements is estimated to be ± 0.3 K, which is more accurate than absolute values due to common errors canceling each other out in the differencing process.

To achieve these goals required an ultrastable radiometer and good mechanical stability of the test package at the various focal points after installation. It was shown in a previous article [4] that a number of measurements were made with the test packages installed at the different focal points, then back on the ground, and then back at the focal points. Such repeatability tests confirmed that the X-band test package and radiometric system met the accuracy requirements stated above for making absolute and differential noise temperature measurements.

Figures 7 and 8 show the X-band test package installed at f1 and f2. Horns of different gains at f1 and f2 were easily achieved by beginning with the 29-dBi horn and systematically removing horn sections to produce a lower gain horn. At both f1 and f2, test package adjustments were used to align the phase centers for the different gain horns to the desired geometric focal points.

Special radiometric calibration techniques were employed, such as (1) correcting for changes in atmospheric

noise contributions due to changes in air temperature and relative humidity and (2) performing periodic real-time calibrations of the radiometric system for measuring noise temperatures. Further details of the microwave performance of these test packages and radiometric techniques used to achieve the desired stability and precision have been reported elsewhere [5].

V. Results

The measurements described above were made at Cassegrain focus f1, intermediate focus f2, and basement focus f3.

For contrasting the two theories, the most interesting measurements were those made at f2, where the shroud surrounds the mirrors. Since there is no shroud in the pedestal room, both methods give the same result for the basement mirrors.

A horn pattern input at f2 is imaged at f1 so measurements made with the same horn gain at f1 and f2 can be differenced to give the noise temperature due only to the BWG portion of the system. A plot of the measured data for the upper BWG (f2 to f1) is compared to both theories in Fig. 9 for horn gains from 25 to 29.8 dB. Obviously, the lower gain horn spills more energy past the mirrors and has a higher noise temperature contribution. Interestingly, both methods do a fairly good job of predicting noise temperatures. For reference, the BWG system was designed to operate with the 29.8-dB gain horn.

References

[1] A. G. Cha and W. A. Imbriale, "A New Analysis of Beam Waveguide Antennas Considering the Presence of the Metal Enclosure," *IEEE Transactions on Antennas and Propagation*, vol. 40, no. 9, pp. 1041–1046, 1992.

[2] R. F. Harrington, *Time-Harmonic Electromagnetic Fields*, New York: McGraw-Hill, Chapter 8, 1961.

[3] W. Veruttipong and M. Franco, "A Technique for Computation of Noise Temperature Due to a Beam Waveguide Shroud," *1993 IEEE AP-S International Symposium*, The University of Michigan at Ann Arbor, pp. 1659–1662, June 1993.

[4] D. A. Bathker, W. Veruttipong, T. Y. Otoshi, and P. W. Cramer, Jr., "Beam Waveguide Antenna Performance Predictions With Comparisons to Experimental Results," *Microwave Theory and Techniques, Special Issue (Microwaves in Space)*, vol. MTT-40, no. 6, pp. 1274–1285, 1992.

[5] T. Y. Otoshi, S. R. Stewart, and M. M. Franco, "Portable Microwave Test Packages for Beam Waveguide Antenna Performance Evaluations," *Microwave Theory and Techniques, Special Issue (Microwaves in Space)*, vol. MTT-40, no. 6, pp. 1286–1293, 1992.

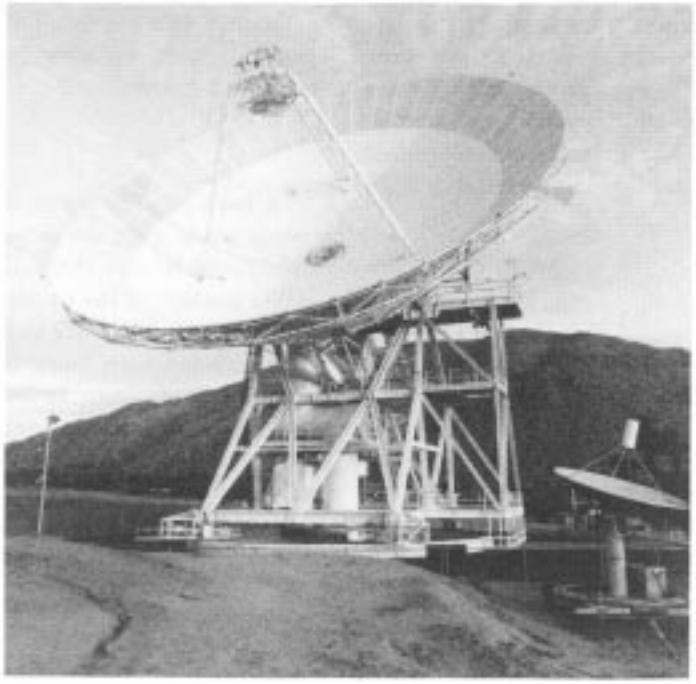

Fig. 1. The DSS-13 34-m BWG antenna.

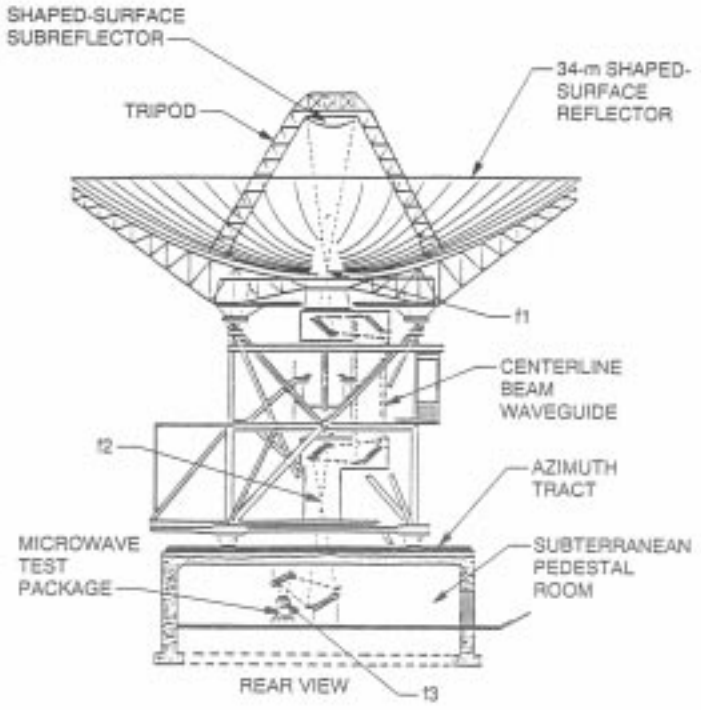

Fig. 2. The 34-m BWG antenna focal points.

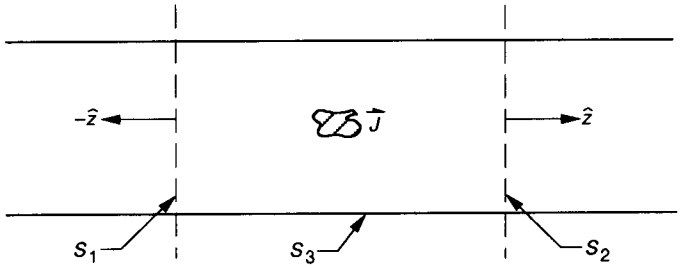

Fig. 3. Geometry for computing waveguide modes.

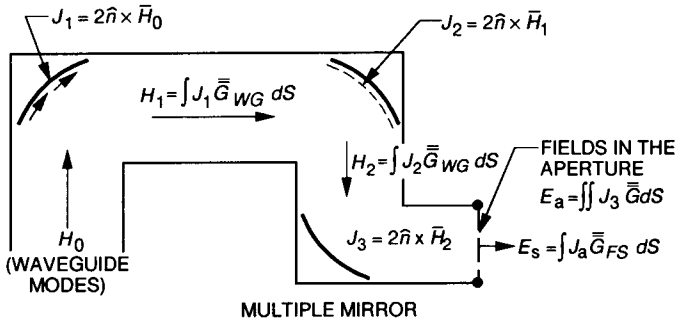

Fig. 4. Computation of fields in the BWG system.

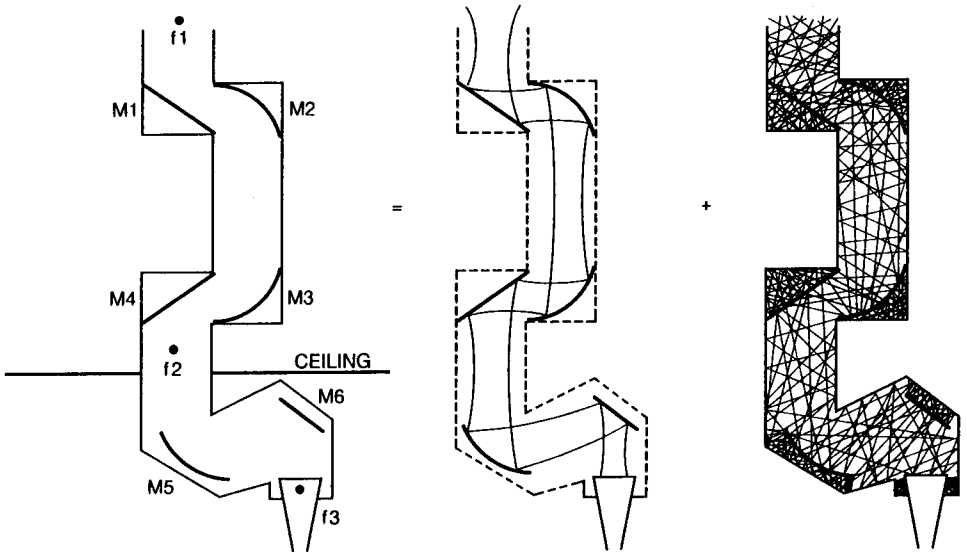

$$P_{BWG} = P_m + P_{spill}$$
$$T_{BWG} = T_m + T_{spill}$$

Fig. 5. Characteristics of the fields inside a BWG shroud and their corresponding noise temperatures.

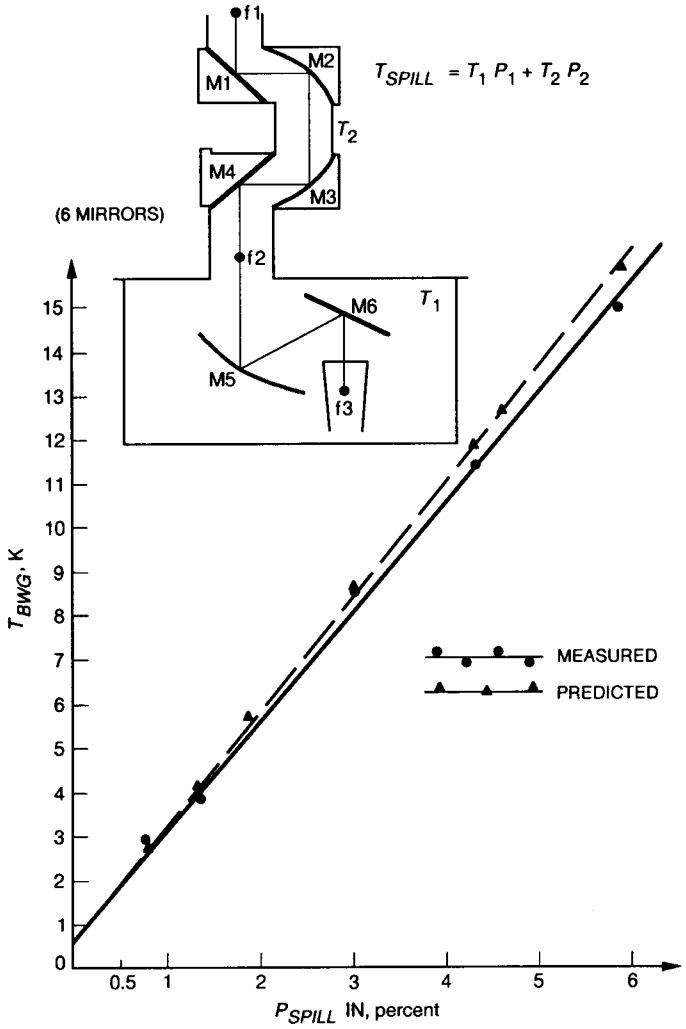

Fig. 6. The comparison between predicted and measured BWG noise temperatures at X-band.

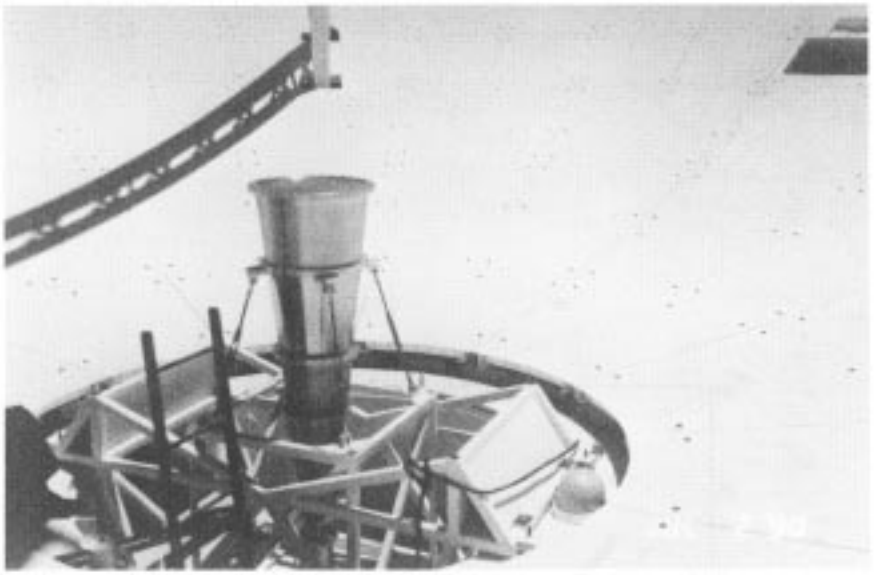

Fig. 7. Partial view of the X-band 29-dBi horn test package and mounting structure installed at the Cassegrain focal point f1.

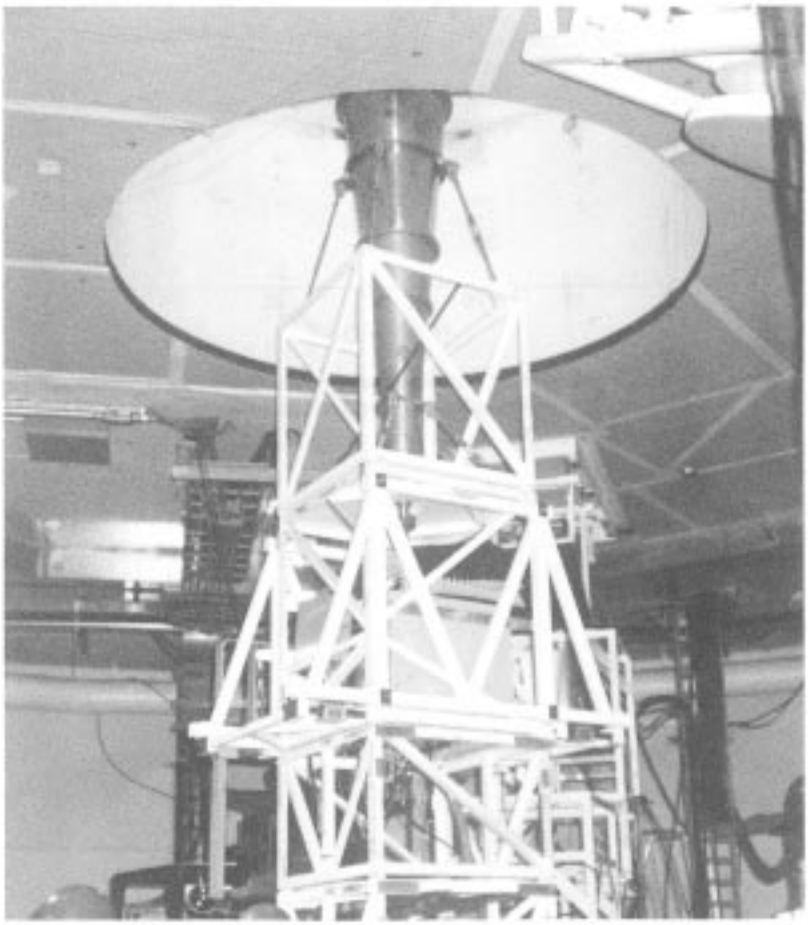

Fig. 8. The 8.45-GHz 22-dBi horn test package and mounting table installed at focal point f2.

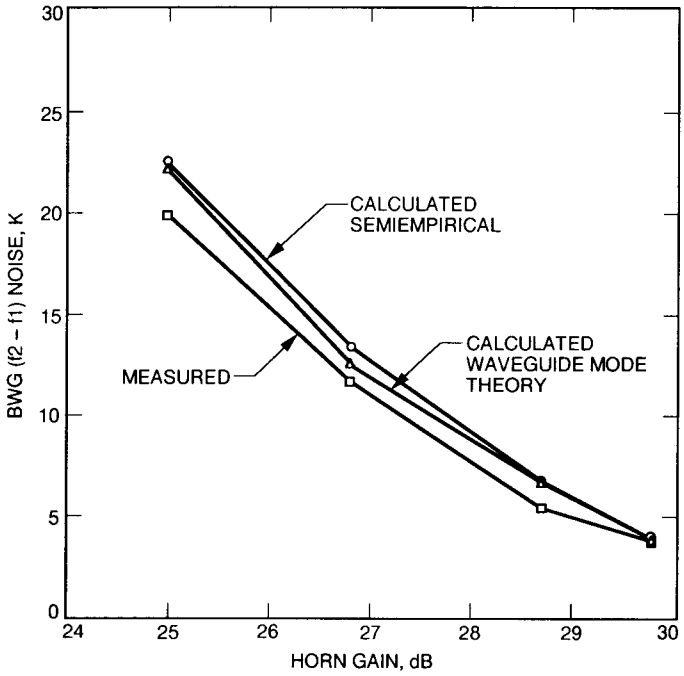

Fig. 9. Comparison of computed and measured noise temperatures with different feedhorn gains at f2.